Phase Behavior and Structure Properties of the Sodium Dodecyl Sulfate (SDS)/ Brij 30/Water System

Hui Yue, Ping Guo, and Rong Guo*

School of Chemistry and Chemical Engineering, Yangzhou University, Yangzhou 225002, People's Republic of China

The phase behavior of the sodium dodecyl sulfate (SDS)/Brij 30/H_2O system is shown by a phase diagram. The system can form micelle, reverse micelle, anisotropic lamellar, and hexagonal liquid crystal regions. The rheological behavior of the viscoselastic solution follows the Maxwell model at lower shear frequencies and deviates from it at higher shear frequencies in the oscillatory frequency sweeping experiment, which is the typical property of wormlike micelles entangled to form a transient network. In addition, the results are evaluated by dynamic light scattering and freeze-fracture images, which are consistent with the rheological behavior.

Introduction

Wormlike micelles, because of their high surface activities and high viscosity, play a very important role in oil−gas exploitation, especially in twice oil extraction.[1−6] It is well-documented that ionic surfactants can form wormlike micelles upon the addition of electrolytes,[7−12] which can decrease the electrostatic interaction among particles so that the size of the micelles increases rapidly, and freely curving aggregations form.

Recently, a lot of research has shown another way to get wormlike micelles: the mixture of surfactants.[13−15] It has been found that different mixed surfactant systems, for example, cationic−anionic, ionic−nonionic, and mixed nonionic surfactant systems can form wormlike micelles. Incorporation of a cosurfactant in the palisade layer of micellar aggregates decreases the average area of the surfactant headgroup, resulting in a decrease in the interfacial curvature of the aggregate. It is, therefore, reasonable to expect one-dimensional micellar growth upon the addition of cosurfactant to the surfactant solution.[16] Polyoxyethylene alkyl ether (C_mEO_n) has been found to be suitable as a lipophilic nonionic cosurfactant. Kunieda and coworkers have investigated the phase behavior of the SDS−$C_{12}EO_n$ system in a water-rich region, and they studied the influence of different EO chain lengths on the formation of wormlike micelles.[15]

In the present paper, we report the phase behavior of a similar system (SDS−$C_{12}EO_4$) and the rheological behavior of wormlike micellar solutions with two different proportions. But, in our experiments, our aim is to learn more about the structural evolution of wormlike micelles such as entanglement, micellar growth, and branching. So, freeze-fractured transmission electron microscopy (FF-TEM) is used to investigate the process of micellar structure changes with different weight ratios of SDS/ $C_{12}EO_4$. Additionally, dynamic light scattering (DLS) is also used.

Experimental Section

Materials. Sodium dodecyl sulfate (SDS, Sigma, 99 %) and Brij 30 (Sigma, > 99 %) were used as received. Water used was deionized and distilled twice.

* Corresponding author. Fax: 86-514-7311374. Tel.: 86-514-7975219. E-mail address: guorong@yzu.edu.cn.

Determination of Partial Phase Diagram. Partial phase diagrams were generated by titration. Samples were prepared in test tubes with caps, mixed on a mixer for several minutes, and then placed in a thermostat at (25 ± 0.1) °C for at least 2 h for phase equilibrium. The monophase region was verified by observing the change from transparent to cloudy when water was dropped into the samples at various weight ratios of SDS/Brij 30 or when Brij 30 was dropped into the samples at various weight ratios of SDS/H_2O. The phase boundaries of the lamellar liquid crystal and hexagonal liquid crystal were verified with a polarizing microscope (59×, Shanghai Photology Apparatus Co., China).

Rheological Measurements. The samples were homogenized and kept in a water bath at (25 ± 0.1) °C for at least 24 h to ensure equilibration before measurements. The rheological measurements were performed in a Rheometer Rheostess RS600 (HAAKE RheoStress) at 25 °C using a cuvette (cup, DG41, 5.100 mm) for low viscosity solutions and cone−plate geometry (diameter 35 mm and cone angle 1°) for highly viscous gels. Frequency sweep measurements were performed in the linear viscoelastic regime of the samples, as determined previously by dynamic strain sweep measurements.

DLS. Measurements were carried out at a scattering angle of 90° using an ALV 5022 laser light scattering (LLS) instrument equipped with a He−Ne laser (model 1145p-3083; output power = 22 mW at λ = 632.8 nm) in combination with an ALV SP-86 digital correlator with a sampling time range of 25 ns to 40 ms. The LLS cell was held in a thermostat index matching vat filled with purified dust-free toluene, with the temperature controlled to ± 0.02 °C. All solutions were filtered through a Millipore filter with a 0.45 μm pore size and thermostatted at 25 °C for at least 0.5 h. The experiment duration was 10 min, and each experiment was repeated at least twice. The intensity time correlation function $G^{(2)}(t, q)$ in the self-beating mode was measured, where t is the decay time and q is the scattering vector ($q = (4\pi n/\lambda_0) \sin(\theta/2)$). $G^{(2)}(t, q)$ can be related to the normalized first-order electric field time correlation function $|g^{(1)}(t, q)|$ via the Siegert relation as[17−19]

$$G^{(2)}(t, q) = A(1 + \beta|g^{(1)}(t, q)|^2) \quad (1)$$

where $A(\equiv \langle I(0)\rangle^2)$ is the measured baseline. For the broadly distributed relaxation spectrum, $|g^{(1)}(t, q)|$ is related to a characteristic relaxation time distribution $G(\tau)$ as

10.1021/je900023t CCC: $40.75
Published on Web 08/21/2009

$$|g^{(1)}(t,q)| \equiv \langle E(0,q)E^*(t,q)\rangle / \langle E(0,q)E^*(0,q)\rangle = \int_0^\infty G(\tau)e^{-t/\tau}d\tau \quad (2)$$

$G(\tau)$ can be calculated from the Laplace inversion of the measured $G^{(2)}(t, q)$ on the basis of eqs 1 and 2 and a translational diffusive coefficient distribution $G(D)$:

$$\Gamma = Dq^2 \quad (3)$$

where $\Gamma = 1/\tau$. The hydrodynamic radius distribution by the Stokes−Einstein equation is:

$$R_h = \kappa_B T/6\pi\eta D \quad (4)$$

where η, k_B, and T are the solvent viscosity, the Boltzmann constant, and the absolute temperature, respectively.

In this study, the CONTIN program supplied with the correlator was used. The intensity-time correlation function from DLS was analyzed by the CONTIN program to give the intensity distribution of particle size in the form $I(\Gamma)$ of decay rate Γ. By using the Stokes−Einstein equation, the intensity distribution of log R_h was calculated.

FF-TEM. For the preparation of replicas, a small amount of sample was placed in a sample cell, which was quickly plunged into liquid nitrogen, and then the frozen samples were fractured and replicated in a freeze-fractured apparatus (Balzers BAF 400D). Replicas were examined with a transmission electron microscope (TEM, Tecnai 12 Philip, Holland).

The temperature for this experiment was kept at (25 ± 0.1) °C.

Results

Partial Phase Diagram. Figure 1a illustrates the partial phase diagram of the SDS/Brij 30/H_2O system. L_1 and L_2 represent micelle and reverse micelle regions, respectively. HEX is the hexagonal liquid crystal region, and LLC is the lamellar liquid crystal region. Figure 1b shows the magnified L_1 region in Figure 1a. The high viscosity region of wormlike micelles in the L_1 region is shown by the shaded area in Figure 1b. The detailed results are described below.

Rheological Behavior

Effect of Brij 30 Content on the Formation of Wormlike Micelles. To study the effect of the Brij 30 concentration on the rheological behavior of SDS micelles, several samples were prepared by adding required amounts of Brij 30 to SDS solutions with the weight ratio of SDS/H_2O at 5:95. Figures 2 and 3 show steady and oscillatory-shear curves of the systems with different Brij 30 contents. The trend is similar to that observed for mixed ionic-nonionic surfactant systems.[13,14,16]

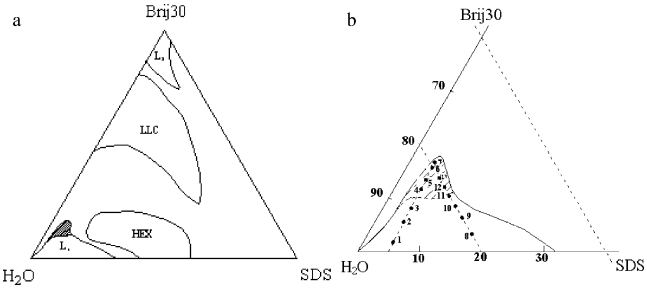

Figure 1. Partial phase diagram for SDS/Brij 30/H_2O system. L_1, micelle consisting of wormlike micelles (shaded area); L_2, reverse micelle; LLC, lamellar liquid crystal; HEX, hexagonal liquid crystal.

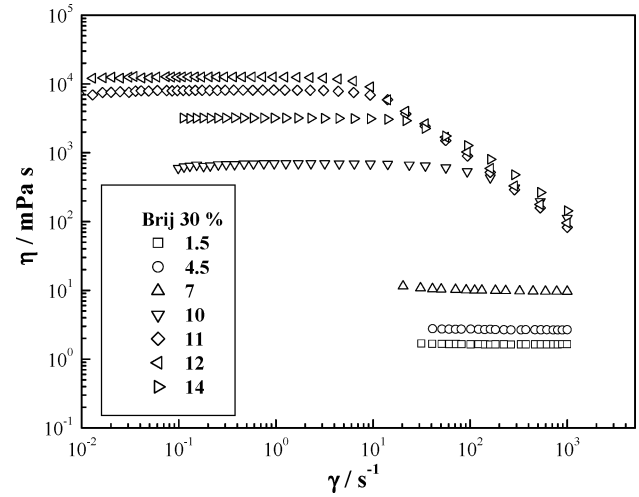

Figure 2. Steady-shear rate viscosity curves for different Brij 30 content at SDS/H_2O = 5:95.

When the Brij 30 content is low (Brij 30 = (1.5, 4.5, 7) % (by weight)), the viscosity of the system is independent of the shear rate. However, when the Brij 30 content is at 10 % (by weight), the viscosity of the system increases sharply, and there is shear thinning when the shear rate is above 10 s^{-1}, which is the typical behavior of wormlike micelles (Figure 2). Further, the viscosity of the sample increases to a maximum value (12.45 Pa·s) when Brij 30 content increases to 12 % (by weight) and then decreases by further increasing the Brij 30 content.

The processes of breaking and reforming of wormlike micelles are determined by the ratio of $\xi = \tau_{break}/\tau_{rep}$, in which τ_{break} is the average waiting time when the micelle with average length L is separated into two parts and τ_{rep} is the time when micelles reform together again. For a quickly separated reaction $\xi = \tau_{break}/\tau_{rep} \ll 1$. There is a single exponential relation:

$$G(t) = G_0 \exp(-t/\tau_R) \quad (5)$$

where G_0 is the plateau modulus, which is given by G' at high ω, and τ_R is the relaxation time. This kind of viscoelastic system is called a Maxwell liquid,[20] in which G', G'', complex viscosity $|\eta^*|$, and ω obey the following relationships:

$$G'(\omega) = G_0 \frac{\omega^2\tau_R}{1 + \omega^2\tau_R^2} \quad (6)$$

$$G''(\omega) = G_0 \frac{\omega\tau_R}{1 + \omega^2\tau_R^2} \quad (7)$$

$$|\eta^*(\omega)| = \frac{(G'^2 + G''^2)^{1/2}}{\omega} \quad (8)$$

When plotting G'' againstG', there should be a semicircle, which is called a Cole−Cole plot. It follows that:

$$(G'')^2 + \left(G' - \frac{G_0}{2}\right)^2 = \left(\frac{G_0}{2}\right)^2 \quad (9)$$

Moreover, the zero-shear viscosity (η_0) is given by the relation:

$$\tau_R = \frac{\eta_0}{G_0} \quad (10)$$

The relaxation time τ_R can be estimated at $(\omega_R)^{-1}$ where ω_R is the frequency at which G' is equal to G''. τ_R is related to the

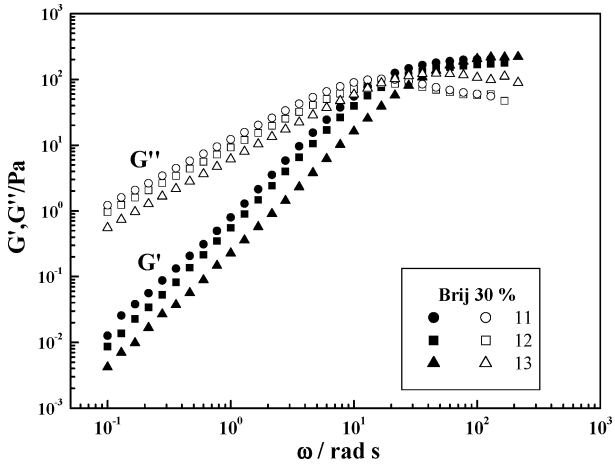

Figure 3. Dynamic rheological behavior for different Brij 30 content at SDS/H_2O = 5:95.

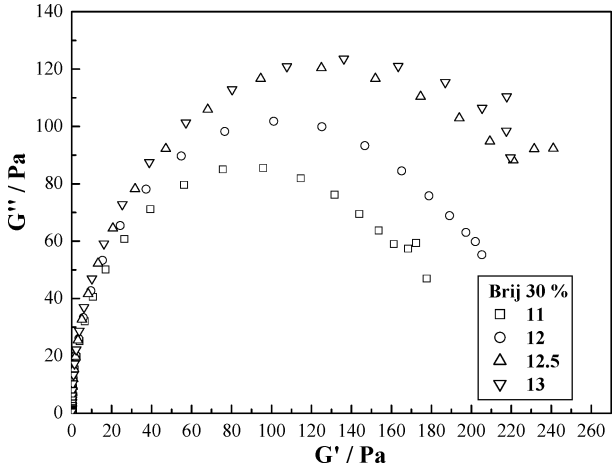

Figure 4. Cole−Cole plot.

microcosmic structure of the materials and is influenced by the composition of the sample, by temperature, and so on.

The dynamic shear curves of the system are shown in Figure 3. When the Brij 30 content is at 11 % (by weight), at low oscillatory shear frequencies the storage modulus G' is smaller than the loss modulus G'', and both G' and G'' increase with sweeping frequency. However, G' and G'' have a crossover when ω_R = 20.45 rad/s, which corresponds to the single relaxation time τ_R = 21.50 s. We can see clearly that the system follows the Maxwell model within the lower shear frequency range (Figure 4) but deviates from Maxwell behavior at higher shear frequencies. ω_R decreases, and the relaxation time τ_R increases when the Brij 30 content increases to 12 % (by weight), and the relaxation time τ_R decreases with a further increase of the Brij 30 content (Figure 5).

Effect of Weight Ratio of SDS/Brij 30 (w/w) on the Formation of Wormlike Micelles. Meanwhile, we also investigated the effect of the weight ratio of SDS/Brij 30 on the rheological behavior of wormlike micelles at a constant water content (80 % (by weight)).

Figure 6 shows that the zero-shear viscosity of the system is constant with SDS/Brij 30 (w/w) changing from 99:1 to 65:35 and then increases slowly in the SDS/Brij 30 (w/w) range of 65:35 to 40:60, and it increases sharply up to a maximum value (12.36 Pa·s) at SDS/Brij 30 (w/w) = 33:67. Finally, the viscosity of the system decreases quickly with SDS/Brij 30.

Figure 7 shows the dynamic shear curve of the system, whose results are similar to those in Figure 3. The Cole−Cole plot of

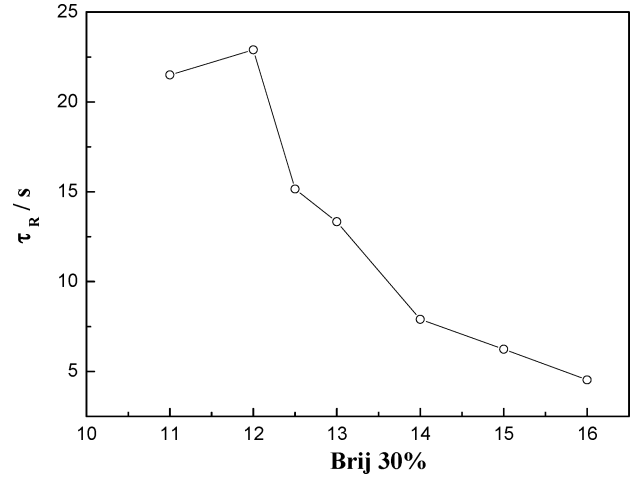

Figure 5. Variation of τ_R as a function of different Brij 30 content at SDS/H_2O = 5:95.

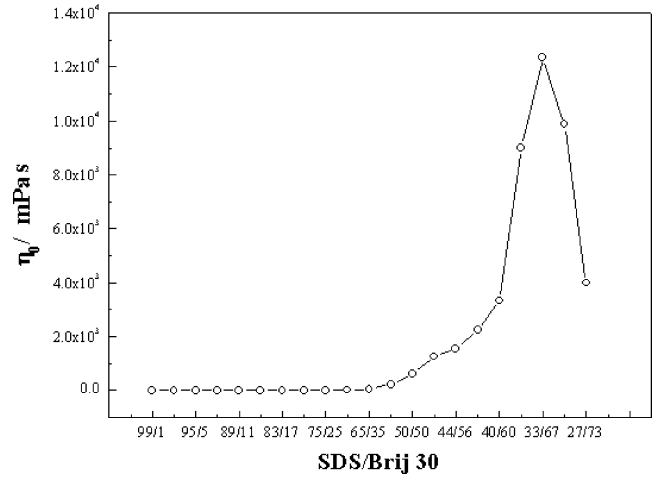

Figure 6. Variation of zero-shear viscosity (η_0) as a function of different SDS/Brij 30 (w/w) at H_2O = 80 % (by weight).

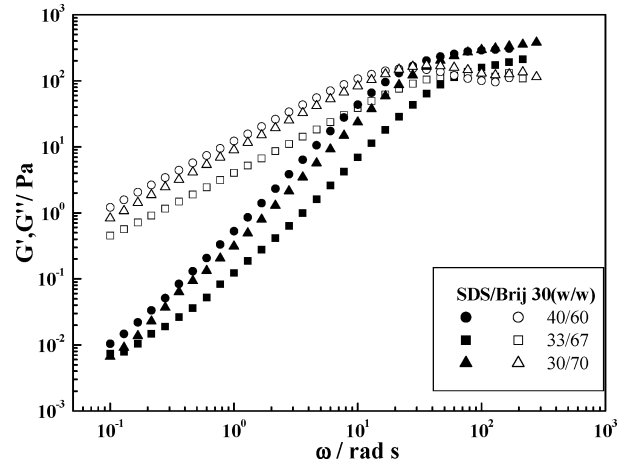

Figure 7. Dynamic rheological behavior for different SDS/Brij 30 (w/w) at H_2O = 80 % (by weight).

the system is shown in Figure 8, from which we can also see the system fits the Maxwell model at lower frequencies and deviates from Maxwell behavior at higher frequencies, which is probably caused by the Rouse model of stress relaxation.[21] Figure 9 shows the change of relaxation time τ_R as a function of SDS/Brij 30 (w/w), which indicates the growing and stress relaxation of the micelles.

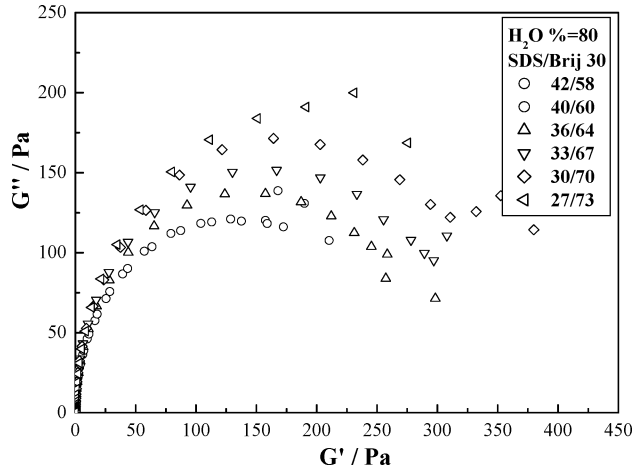

Figure 8. Cole−Cole plot according to frequency sweep.

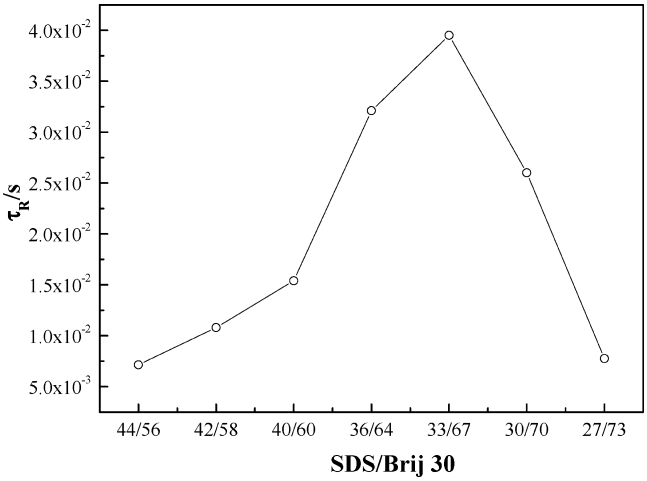

Figure 9. Variation of τ_R as a function of different SDS/Brij 30(w/w) at H_2O = 80 % (by weight).

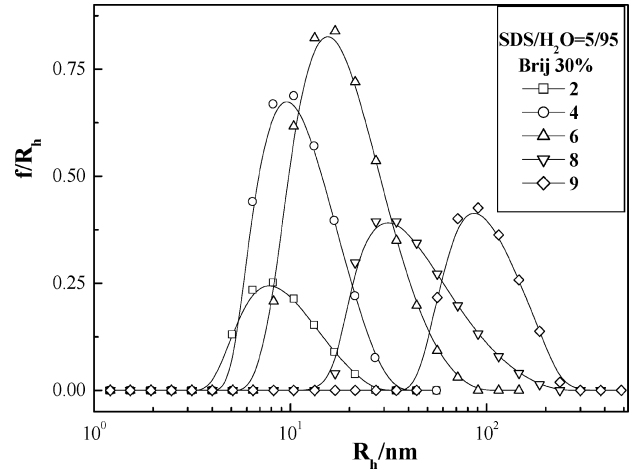

Figure 10. Normalized hydrodynamic radius (R_h) distributions of different Brij 30 % (by weight) at SDS/H_2O = 5:95.

Size and Images of Wormlike Micelles. Figures 10 and 11 show the hydrodynamic radius distributions of mixed micelles with different Brij 30 contents at a constant weight ratio of SDS/H_2O (5:95) and with different ratios of SDS/Brij 30 at a constant weight ratio of water (80 %), respectively.

From Figure 10 and Table 1, we can see that at weight ratio SDS/H_2O = 5:95, SDS and Brij 30 form mixed spherical micelles with $\langle R_h \rangle \approx$ 7.71 nm at Brij 30 = 2 % (by weight),

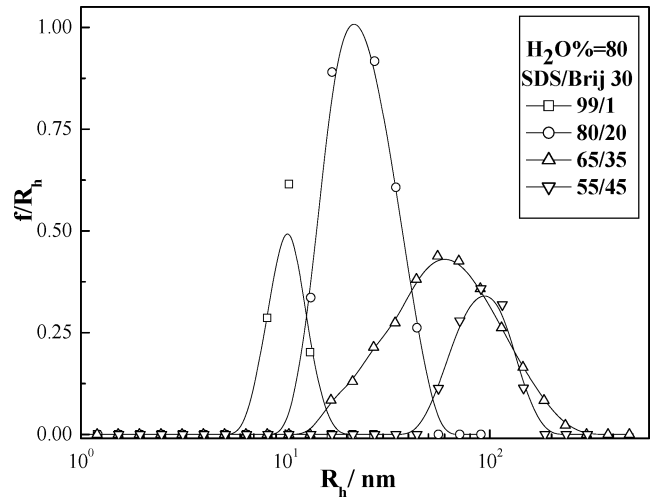

Figure 11. Normalized hydrodynamic radius (R_h) distributions of different SDS/Brij 30 (w/w) at H_2O = 80 % (by weight).

Table 1. Normalized Hydrodynamic Radius (R_h) Distributions of Different Brij 30 % (by Weight) at SDS/H_2O = 5:95

Brij 30	R_h
% (by weight)	nm
2	7.71
4	10.26
6	18.44
8	41.16
9	80.65

and the FF-TEM images of micelle are shown in sample 1 in Figure 12. By further increasing Brij 30 (6 % (by weight)), the spherical micelles grow and even assemble together to form short rod-like micelles with $\langle R_h \rangle \approx$ 18.44 nm (sample 2 in Figure 12), and short rod-like micelles form long rod-like micelles with $\langle R_h \rangle \approx$ 41.16 nm at Brij 30 = 8 % (by weight) and $\langle R_h \rangle \approx$ 80.65 nm at Brij 30 = 9 % (by weight) (sample 3 in Figure 12).

By further increasing Brij 30 to 11 % (by weight), long rod-like micelles entangle with each other and form wormlike micelles (sample 4 in Figure 12). Now, the solution is so viscous that it cannot filter through the Millipore filter, so that the size of micelle aggregates in the solution is not measured by DLS.

When the content of Brij30 is 12 % (by weight), there are orderly arranged wormlike micelles (sample 5 in Figure 12). However, wormlike micelles begin branching (sample 6 in Figure 12) with the percentage of Brij 30 increasing to 13 % (by weight), and wormlike micelles branch seriously when Brij 30 content increases to 16 % (by weight) (sample 7 in Figure 12).

Also, when fixing water content at 80 % (by weight), Figure 13 and Table 2 indicate that SDS and Brij 30 form spherical micelles with $\langle R_h \rangle \approx$ 10.74 nm at SDS/Brij 30 (w/w) = 90:10 (sample 8, Figure 13), spherical micelles grow to $\langle R_h \rangle \approx$ 23.41 nm at SDS/Brij 30 (w/w) = 83:17 (sample 9 in Figure 13), and short rod-like micelles assemble together to form long rod-like micelles with $\langle R_h \rangle \approx$ 57.13 nm at SDS/Brij 30 (w/w) = 65:35 (sample 10 in Figure 13). Further, long rod-like micelles entangle with each other, and wormlike micelles begin to form with $\langle R_h \rangle \approx$ 98.25 nm at SDS/Brij 30 (w/w) = 50:50 (sample 11 in Figure 13).

Wormlike micelles are formed by further increasing Brij 30 content (sample 12 in Figure 13), and when SDS/Brij 30 (w/w) = 33:67, there are orderly arranged networks (sample 13 in

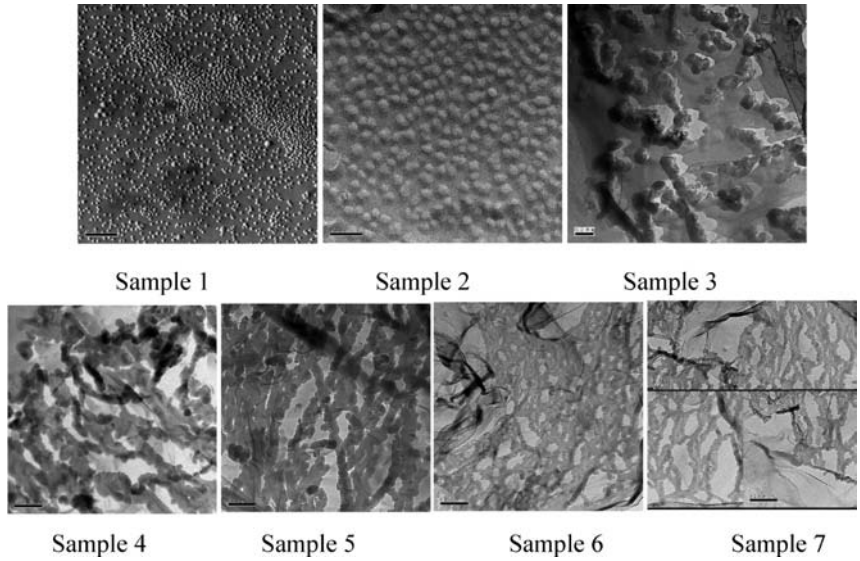

Figure 12. Freeze-fractured images of micelles aggregates. The compositions of samples 1 to 7 are the same as those in Figure 1b.

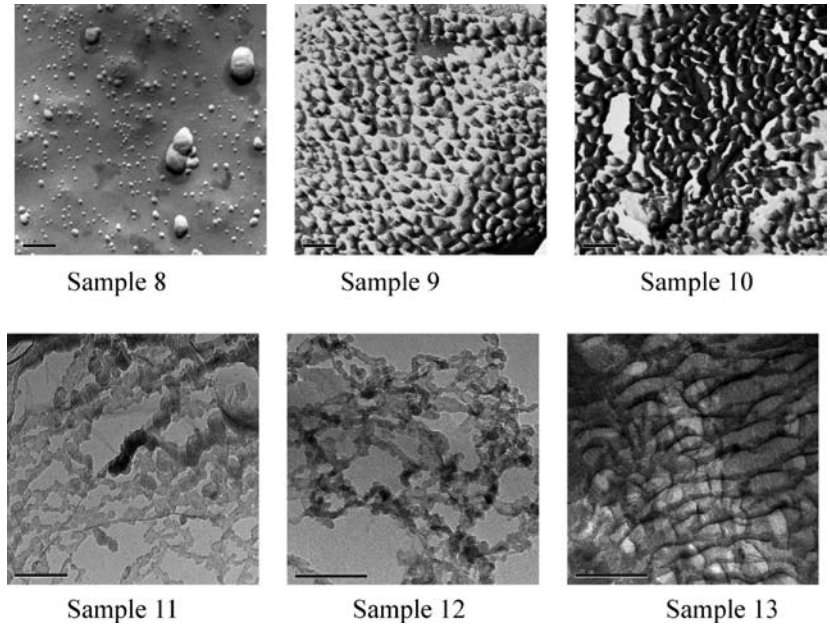

Figure 13. Freeze-fractured images of micelles aggregates. The compositions of samples 8 to 13 are the same as those in Figure 1b.

Table 2. Normalized Hydrodynamic Radius (R_h) Distributions of Different SDS/Brij 30 (w/w) at H_2O = 80 % (by Weight)

SDS/Brij 30 (w/w)	R_h nm
90:10	10.74
83:17	23.41
65:35	57.13
50:50	98.25

Figure 13). However, if Brij 30 keeps increasing, we can see branching wormlike micelles from sample 6 in Figure 12.

Discussion

View Obtained from Steady-State Experiments. In steady-state experiments, when the Brij 30 content is low, SDS and Brij 30 form spherical mixed micelles by electrostatic interaction and hydrophobic interaction (Table 1, sample 1 in Figure 12). The system exhibits Newtonian fluid behavior, and the viscosity is independent of shear rate. By increasing Brij 30, short rod-like micelles are formed, and then they assemble together to form long rod-like micelles (Table 1, sample 2 in Figure 12). When the viscosity increases the system still shows Newtonian fluid behavior. When Brij 30 = 11 % (by weight), long rod-like micelles entangle with each other, and wormlike micelles are formed (sample 4 in Figure 12). The viscosity of the system increases sharply, and there is shear thinning when the shear rate is above 10 s^{-1} (Figure 2). This is the typical behavior of wormlike micelles. When the shear rate is larger than the critical shear rate, the viscosity decreases because of the breaking of the structured networks. By further increasing Brij 30, the networks become more compact, and the critical shear rate shifts to lower values. We can still see that, when the concentration of Brij 30 is above a critical concentration, such as Brij 30 = 12 % (by weight), the micelles start to entangle with each other, a network (sample 5 in Figure 12) is formed, and the viscosity of the system increases due to hindered diffusion of entangled micelles. When the concentration of Brij 30 in the system comes to a certain value[22,23] the viscosity of the system decreases by further increasing Brij 30, which shows

a structural change in the system or branching of micelles (sample 6 and 7 in Figure 12).

The variation of zero-shear viscosity (η_0) as a function of the ratio of SDS/Brij30 further shows the existence of wormlike micelles (Figure 6). When the Brij 30 content is low, SDS and Brij 30 form spherical mixed micelles (Table 2, sample 8 in Figure 13), and the viscosity is small. Then micelles grow, and rod-like micelles are formed; η_0 increases sharply with increasing weight ratio of SDS/Brij30 (samples 9 and 10 in Figure 13). When the concentration of Brij30 is above a critical concentration (SDS/Brij 30 (w/w) = 50:50), the micelles start to entangle with each other, and wormlike micelles are formed (sample 11 in Figure 13); the viscosity of the system increases due to hindered diffusion of entangled micelles. Further, the micelle becomes the longest, which leads to a maximum value of η_0 by further increasing Brij 30 (SDS/Brij 30 (w/w) = 33:67), and orderly wormlike micelles are obtained (Figure 13). Then, η_0 decreases due to the breaking or branching of the micelles.[24−26]

View Obtained from Dynamic Experiments. The dynamic shear curves of the system are shown in Figures 3 and 7. At lower oscillatory shear frequencies, the storage modulus G' is smaller than the loss modulus G'', and the system shows a liquid-like behavior and follows the Maxwell model in this region. At higher shear frequencies, G' exceeds G''. However, G' does not attain a well-defined plateau modulus G_0, and there is no minimum of G'', which indicates the system deviates from Maxwell behavior; there are various processes of stress relaxation.

The deviations from Maxwell behavior are better illustrated by Cole−Cole plots (Figures 4 and 8). The low-frequency data obtained with eq 9 best fit semicircles. It can be noticed that deviations from oscillating semicircles occur throughout the surfactant domain, meaning that the condition for the fast breaking limit is not completely fulfilled. Stronger departures are found at low surfactant concentrations, where non-Maxell behavior starts at moderate frequencies. As the Brij 30 concentration increases or the weight ratio of SDS/Brij 30 increases, deviations from semicircles are less significant and take place at higher frequencies. The original radius of these oscillating semicircles increases steadily with surfactant concentration, implying an increase in the shear modulus. So, the system fits the Maxwell model at low frequencies and deviates from Maxwell behavior at high frequencies, which is probably caused by the various processes of stress relaxation.

On the other hand, ω_R decreases, and the relaxation time τ_R increases by increasing the Brij30 content or the decreasing of the weight ratio of SDS/Brij 30. The rheology changes of the system are caused by the increasing of the micelle length and the network density. Then, by further increasing of Brij 30 or decreasing of the weight ratio of SDS/Brij 30, the relaxation time τ_R decreases again because of the decrease of the networks.

The changes of τ_R as a function of Brij30 (Figures 5 and 9) are the same as the change of zero-shear viscosity (Figure 6). As can be seen from the curve, by increasing Brij30, τ_R increases due to a rapid increase of wormlike micelles. By further increasing Brij30, τ_R decreases. Such a behavior may have originated from the fusion of the free ends of the aggregate with the cylindrical parts of the micelles. Thus micellar joints are formed where fast stress relaxation can occur by sliding of the connection point along the cylindrical body.[27]

So, whether we fix SDS/H_2O (w/w) = 5:95 with changing Brij 30 % (by weight) or H_2O = 80 % (by weight) with different weight ratios of SDS/Brij 30 (w/w), micelles change as follows: spherical micelles → short rod-like micelles → long rod-like micelles → wormlike micelles → branching wormlike micelles, with increasing Brij 30 content in the system.

It is clear that Brij 30 is helpful to the formation of wormlike micelles because the exit of Brij 30 may prevent the repulsion function of polarity headgroup in SDS molecules, and hydrobond interaction of the headgroup in Brij 30 molecules is helpful to forming more ordered micelle aggregates. However, it is also very important for us to know that it is not right that the greater Brij 30 content is, the easier it is to form wormlike micelles. There is an appropriate content of SDS and appropriate proportion for SDS and Brij 30 to form wormlike micelles (Figure 13).

Conclusion

The SDS/Brij 30/H_2O system can form wormlike micelles. Addition of Brij 30 reduces the average area of surfactant headgroup and induces one-dimensional micellar growth. With successive addition of Brij 30, viscosity increases rapidly to form viscoelastic solutions and then decreases after the maximum, and ultimately, a phase separation occurs. The rheological behavior of viscoselastic solutions follow the Maxwell model at lower shear frequencies; however, at higher shear frequencies they deviate from the Maxwell model, which are the typical properties of wormlike micelles entangled to form a transient network. Measurements of DLS and freeze-fracture images indicate the existence of wormlike micelles as well as the changing of micelle aggregates while increasing Brij 30. These results are consistent with the rheological behavior.

Literature Cited

(1) Jiang, Y. Cryo-TEM studies of worm-like micellar solutions. *Curr. Opin. Colloid Interface Sci.* **2002**, *7*, 276–281.

(2) Raghavan, S. R.; Kaler, E. W. Highly Viscoelastic Wormlike Micellar Solutions Formed by Cationic Surfactants with Long Unsaturated Tails. *Langmuir* **2001**, *17*, 300–306.

(3) Schubert, B. A.; Kaler, E. W.; Wagner, N. J. The Microstructure and Rheology of Mixed Cationic/Anionic Wormlike Micelles. *Langmiur* **2003**, *19*, 4079–4089.

(4) Jadzyn, D. R.; Lech, T.; Czechowski, G. Viscosity of the Homologous Series of *n*-Alkylcyanobiphenyls. *J. Chem. Eng. Data* **2001**, *46*, 110–112.

(5) Acharya, D. P.; Kunieda, H. Formation of viscoelastic wormlike micellar solutions in mixed nonionic surfactant systems. *J. Phys. Chem. B* **2003**, *107*, 10168–10175.

(6) Koehler, R. D.; Raghavan, S. R.; Kaler, E. W. Microstructure and Dynamics of Wormlike Micellar Solutions Formed by Mixing Cationic and Anionic Surfactants. *J. Phys. Chem. B* **2000**, *104*, 11035–11044.

(7) Gelbart, W. M.; Ben-Shaul, A.; Roux, D. *Micelles, Membranes, Microemulsions and Monolayers*; Springer: New York, 1994; Chapters 1 and 2.

(8) Porte, G.; Appel, J.; Poggi, J. Experimental investigations on the flexibility of elongated cetylpyridinium bromide micelles. *J. Phys. Chem.* **1980**, *84*, 3105–3110.

(9) Missel, P. J.; Mazer, N. A.; Benedek, G. B.; Young, C. Y.; Carey, M. C. Thermodynamic analysis of the growth of sodium dodecyl sulfate micelles. *J. Phys. Chem.* **1980**, *84*, 1044–1057.

(10) Angelescu, D.; Khan, A.; Caldararu, H. Viscoelastic properties of sodium dodecyl sulfate with aluminum salt in aqueous solution. *Langmuir* **2003**, *19*, 9155–9161.

(11) Croce, V.; Cosgrove, T.; Dreiss, C. A. Giant micellar worms under shear: A rheological study using SANS. *Langmuir* **2005**, *21*, 6762–6768.

(12) Michel, E.; Porte, G.; Cipelletti, L.; Appell, J. Analysis by the two-fluids model of the dynamical behavior of a viscoelastic fluid probed by dynamic light scattering. *Langmuir* **2004**, *20*, 984–999.

(13) Rodriguez, C.; Acharya, D. P.; Hattori, K.; Sakai, T.; Kunieda, H. Phase and Rheological Behavior of Surfactant/Novel Alkanolamide/Water Systems. *Langmuir* **2003**, *19*, 8692–8696.

(14) Acharya, D. P.; Hattori, K.; Sakai, T.; Kunieda, H. Phase and Rheological Behavior of Salt-Free Alkyltrimethylammonium Bromide/Alkanoyl-*N*-methylethanolamide/Water Systems. *Langmuir* **2003**, *19*, 9173–9178.

(15) Acharya, D. P.; Sato, T.; Kaneko, M.; Singh, Y.; Kunieda, H. Effect of Added Poly(oxyethylene)dodecyl Ether on the Phase and Rheo-

logical Behavior of Wormlike Micelles in Aqueous SDS Solutions. *J. Phys. Chem. B* **2006**, *110*, 754–760.
(16) Acharya, D. P.; Kunieda, H. Wormlike micelles in mixed surfactant solutions. *Adv. Colloid Interface Sci.* **2006**, *123*, 401–413.
(17) Provencher, S. W. A Fourier method for the analysis of exponential decay curves. *Biophys. J.* **1976**, *16*, 27–41.
(18) Provencher, S. W. An eigenfunction expansion method for the analysis of exponential decay curves. *J. Chem. Phys.* **1976**, *64*, 2772–2777.
(19) Berne, B. J.; Pecora, R. *Dynamic light scattering*; New York: Plenum Press, 1976.
(20) Rehage, H.; Hoffmann, H. Rheological properties of viscoelastic surfactant systems. *J. Phys. Chem.* **1988**, *92*, 4712–4719.
(21) Suksamranchit, S.; Sirivat, A.; Jamieson, A. M. Influence of polyethylene oxide on the rheological properties of semidilute, wormlike micellar solutions of hexadecyltrimethylammonium chloride and sodium salicylate. *J. Colloid Interface Sci.* **2006**, *304*, 497–504.
(22) Kern, F.; Lequeux, F.; Zana, R.; Candau, S. J. Dynamical pmperies of salt-free viscoelastic micellar solutions. *Langmuir* **1994**, *10*, 1714–1723.
(23) Magid, L. J. The surfactant-polyelectrolyte analogy. *J. Phys. Chem. B* **1998**, *102*, 4064–4074.
(24) Hassam, P. A.; Ragnavan, S. R.; Eric, W. K. Microstructure change in SDS micelles induced by hydrotropic salt. *Langmuir* **2002**, *18*, 2543–2548.
(25) Drye, T. J.; Cates, M. E. Living networks—the role of cross-links in entangled surfactant solutions. *J. Chem. Phys.* **1992**, *96*, 1367–1375.
(26) Lequeux, F. Reptation of Connected Wormlike Micelles. *Europhys. Lett.* **1992**, *19*, 675–681.
(27) Candau, S. J.; Oda, R. Linear viscoelasticity of salt-free wormlike micellar solutions. *Colloids Surf., A* **2001**, *183*, 5–14.

Received for review January 7, 2009. Accepted July 26, 2009. This research work was supported by the National Nature Science Foundation of China (Nos. 20633010 and 20773106).

JE900023T